water MDPI

Article

Experimental Study of Mesostructure Deformation Characteristics of Unsaturated Tailings with Different Moisture Content

Weile Geng [1,2], Wensong Wang [1,*], Zuoan Wei [1,*], Gun Huang [1], Xiaofei Jing [3], Changbao Jiang [1] and Sen Tian [1]

1 State Key Laboratory of Coal Mine Disaster Dynamics and Control, School of Resources and Safety Engineering, Chongqing University, Chongqing 400044, China; gwle@cqu.edu.cn (W.G.); hg023@cqu.edu.cn (G.H.); jcb@cqu.edu.cn (C.J.); sentian@cqu.edu.cn (S.T.)
2 School of Safety and Environment Engineering, Hunan Institute of Technology, Hengyang 421002, China
3 School of Safety Engineering, Chongqing University of Science and Technology, Chongqing 401331, China; xfjing@cqust.edu.cn
* Correspondence: wws@cqu.edu.cn (W.W.); weiza@cqu.edu.cn (Z.W.)

Abstract: A portion of the accumulated tailings in a tailings pond exhibits an unsaturated state. The mechanical properties of unsaturated tailings affect the safety and stability of tailings dams. To investigate the effect of moisture content on the deformation characteristics of unsaturated tailings in the mesoscale, a special testing apparatus is applied to experimentally study the settlement deformation and mesostructure evolution of unsaturated tailings under continuous load. The results show that the mesostructure deformation of unsaturated tailings with different moisture contents under load is the same and can be divided into four stages: pore compression, elastic deformation, structure change, and further compaction. However, the critical pressures of the four stages are significantly different; there is an optimal moisture content corresponding to the maximum deformation resistance. Moreover, the influence of the liquid bridge regime on the mesostructure deformation of unsaturated tailings is discussed in this paper.

Keywords: unsaturated tailings; mesostructure deformation; moisture content; confined compression test; degree of saturation

Citation: Geng, W.; Wang, W.; Wei, Z.; Huang, G.; Jing, X.; Jiang, C.; Tian, S. Experimental Study of Mesostructure Deformation Characteristics of Unsaturated Tailings with Different Moisture Content. *Water* **2021**, *13*, 15. https://dx.doi.org/10.3390/w13010015

Received: 25 November 2020
Accepted: 21 December 2020
Published: 24 December 2020

1. Introduction

Tailings are granular solid waste generated from the production activities of metal and nonmetal mines, which are generally stored by constructing tailings dams to form tailings ponds [1,2]. A tailings dam failure causes serious damage to the surrounding environment and ecosystem, and severe loss of lives and property of downstream residents [3–6]. For example, the Feijão tailings dam in Brumadinho, Minas Gerais, Brazil, collapsed on 25 January 2019, causing 259 deaths and 11 missing person cases [7]. Furthermore, approximately 10 million cubic meters of tailings–water mixtures flowed into the surrounding streams and rivers, causing serious ecological and environmental damage [8,9]. According to statistics, there have been approximately 50 tailings dam accidents in the past 20 years, and the frequency of accidents is on the rise [10].

Currently, China has more than 12,000 tailings ponds, of which approximately 95% are constructed using upstream methods [11]. In this method, tailings slurry, a mixture of solid tailings and tail water, is discharged into a reservoir from the crest of the dam, which forms a deposited beach with a certain slope under the action of gravity. The part of the deposited beach near the crest of the dam is called the dry beach, which is not covered by tail water and becomes the foundation of the embankment in the next stage. Figure 1 depicts a photograph of a tailings pond in southwest China that shows the different positions, such as the embankment, dry beach, water pond, and dam crest, of a tailing dam.

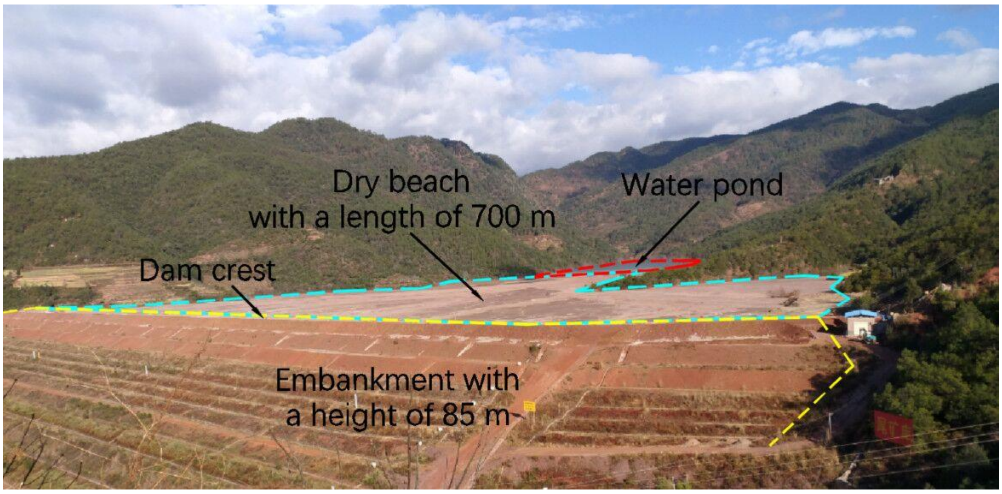

Figure 1. Tailings pond in southwest China.

Figure 2 shows a schematic of an upstream tailings dam structure. The accumulated tailings are divided into unsaturated and saturated portions via the seepage line inside the tailings dam. The mechanical parameters of rock and soil are related to the moisture content (degree of saturation) [12]. The presence of water in the pores and fissures inside the rock and soil weakens their strength. Several landslides and dam collapse accidents are related to pore water. The investigations show that in a tailings dam constructed using the upstream method, the unsaturated tailings above the seepage line account for approximately 10% of the total accumulated tailings, with a high degree of saturation, which generally exceeds 50% [13–15]. Moreover, after the tailings pond becomes inactive, the unsaturated zone in the tailings pond is generally expanded further. The high degree of saturation in the unsaturated zone of a tailings dam is mainly caused by the continuous addition of water from the slurry discharge, as well as capillary rise and rainfall [13]. This significantly affects the stability of the tailings dam [16,17], particularly during earthquakes and vibrations caused by mining activities [18]. For example, the reduction in the strength of tailings in unsaturated zones due to improper pore water management and high and intense regional wet season rainfall is a primary reason for the Feijão tailings dam disaster in 2019 [19]. Therefore, it is critical to study the influence of moisture content on the mechanical properties of unsaturated tailings.

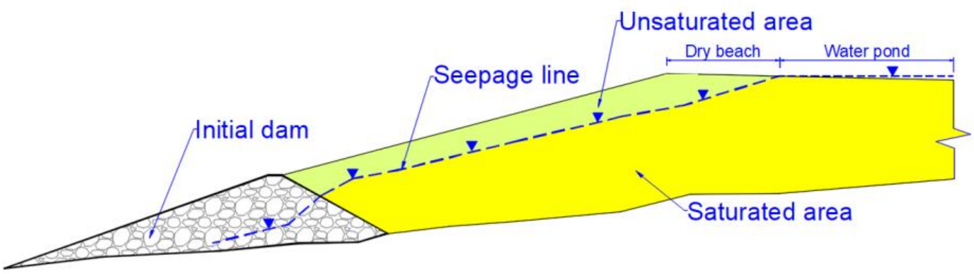

Figure 2. Schematic of an upstream tailings dam structure.

Recently, several studies investigated the strength and deformation characteristics [20–22], permeability [16,23,24], wave velocity [21], and water evaporation laws [25] of unsaturated tailings. However, these studies were performed at a macroscale, regardless of whether the method was employed in a laboratory experiment, field in situ experiment, or numerical simulation. Particularly, the macroscopic properties of tailings are determined in nature on a smaller scale, such as the connection structure of the particles. Tailings have significant dispersion and uneven internal particle structure distribution. With the development of plasticity, the characteristics of discontinuous media are more prominent under load [26]. Conventional research on the macroscopic nature cannot reflect this characteristic. The research scale of the tailing particle structure was called the microscale in the past. Presently, the research scale for soil particle and pore structure morphology and evolution is widely recognized as the mesoscale [27–31], which is between the macroscale (incremental stress and strain) and microscale (contact force and contact displacement) [32,33]. A constant rise in the tailings dam leads to a constant change in the stress conditions of the tailings accumulated in the tailings pond. The changes in the mesostructure of the tailings under load cause their macroscopic deformation and destruction as well as changes in the mechanical properties, which are the predominant causes for tailings dam failure [34]. However, the existing studies on the mesoscopic nature of tailings were mainly performed under saturated conditions using physical experiments [35–37] or discrete element method (DEM) numerical simulations [38]. Few studies reported the mesostructure evolution of unsaturated tailings particles under load.

In summary, the moisture content (degree of saturation) significantly affects the mechanical properties of the tailings, which affect the safety and stability of tailings dams. However, few studies investigate the influence of moisture content on the deformation and structure evolution of tailings in the mesoscopic scale. The particle morphology of tailings is significantly different from that of natural soils [39]. Thus, the particle structure deformation characteristics of unsaturated tailings under load may be different from those of the natural soils. We considered the studies regarding mesomechanics of granular material [40] and used a special testing apparatus to experimentally study the mesostructure deformation characteristics of tailings with different moisture contents. The results are of vital for understanding the deformation and failure mechanisms of unsaturated tailings under load.

Therefore, the objectives of this work are twofold: to study the settlement displacement and mesostructure deformation of unsaturated tailings under continuous load; to examine the influence of moisture content on the settlement characteristics and mesostructure evolution law of tailings.

2. Test Materials, Equipment, and Method

2.1. Test Materials

As shown in Figure 3, the test tailings were the latest produced tailings collected from the discharge pipe of the Huangcaoping tailings pond that belongs to Pingchuan Iron Co., Ltd., Sichuan Province, China. The tailings particle size distribution, shown in Figure 4, was determined using a S3500 light-scattering particle size analyzer (manufactured by Microtrac, Inc., Montgomeryville, PA, USA). The parameters of particle size distribution characteristic and certain other physical properties are listed in Table 1. The test tailings can be classified as tailings silt according to the China National Standard GB50863 [41] and sandy silty clay according to the American Society of Testing Materials Standard D2487 [42].

(**a**) (**b**)

Figure 3. Tailings sample used in this study: (**a**) raw sample from the tailings pond; (**b**) sample after drying and crushing.

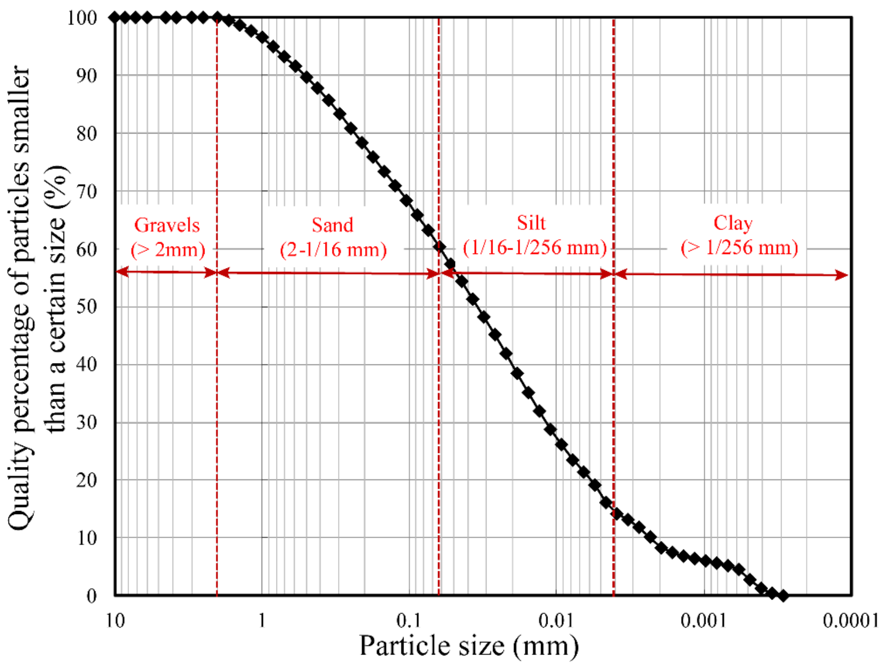

Figure 4. Particle size distribution of the tailings.

Table 1. Particle size distribution parameters and main physical properties of the tailings sample.

Specific Gravity	Liquid Limit (%)	Plastic Limit (%)	Plastic Index	Gravel (%)	Sand (%)	Silt (%)	Clay (%)	D_{50} (mm)	C_u	C_c
2.07	16.97	10.67	6.30	0	39.52	46.04	14.44	0.032	26.03	0.84

Note: D_{50} refers to the average particle size, C_u refers to the uniform coefficient, and C_c refers to the curvature coefficient.

The mineralogical composition of the tailings was analyzed by the Smartlab X-ray diffractometer (XRD) (manufactured by Rigaku Corporation, Tokyo, Japan). The results are shown in Figure 5. The primary minerals in the tailings were quartz, calcite, dolomite, magnetite, chlorite, apatite, and kaolinite.

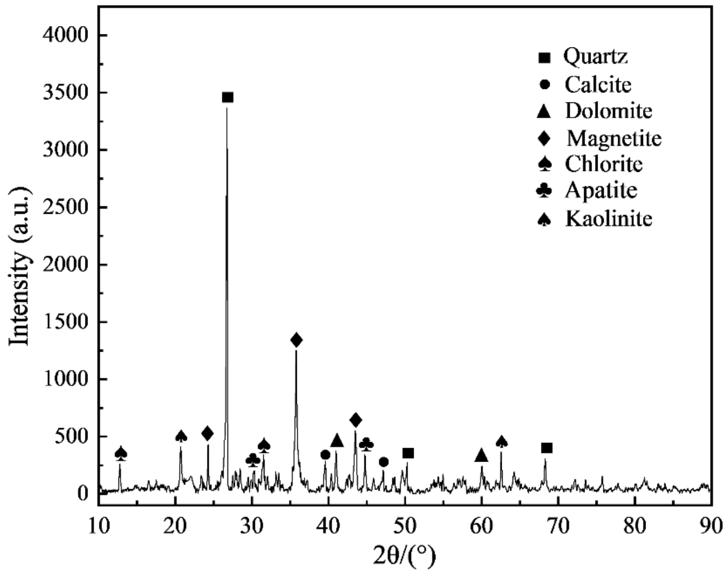

Figure 5. XRD patterns of the tailings.

2.2. Test Equipment

The test equipment is a testing apparatus, developed by us, to observe the mesomechanics and deformation of tailings, as shown in Figure 6a. It is mainly composed of a loading test machine, pressure chamber and accessories, as well as a mesoscopic observation system. Figure 6b shows a schematic of the device structure. Its composition structure and technical parameters are described in detail in [36,37]. This study employs a confined compression test under continuous load, and the loading equipment is an AG–250kNI material testing machine (manufactured by Shimadzu Corporation, Kyoto, Japan).

2.3. Test Scheme

To study the effect of moisture content on the particle structure and mesomechanical behavior of tailings, unsaturated tailings samples with moisture contents of 9%, 12%, 15%, 18%, and 21% were synthesized. The moisture contents were synthesized and verified with the following steps:

(i) Preparation of the dry tailings. According to the geotechnical test technical specification in China (GB/T 50123-2019), the tailings were placed in an oven at 105 °C to dry; no longer changes in the weight of tailings indicated that it had reached a dry state.

(ii) Synthesis of wet tailings with different moisture content. A proper amount of distilled water was mixed with the dry tailings and stirred evenly to synthesize wet tailings with different moisture content. For example, for the sample with a moisture content of 9%, the mass of the distilled water was 9% of the mass of the corresponding dry tailings. To ensure that the moisture content was uniform within the sample, the samples were placed in a sealed bag for 24 h.

(iii) Verification of moisture contents. A small amount of synthesized wet tailings were dried, and the moisture content was calculated; the calculated moisture contents were compared with the required moisture contents to verify the moisture contents of the samples.

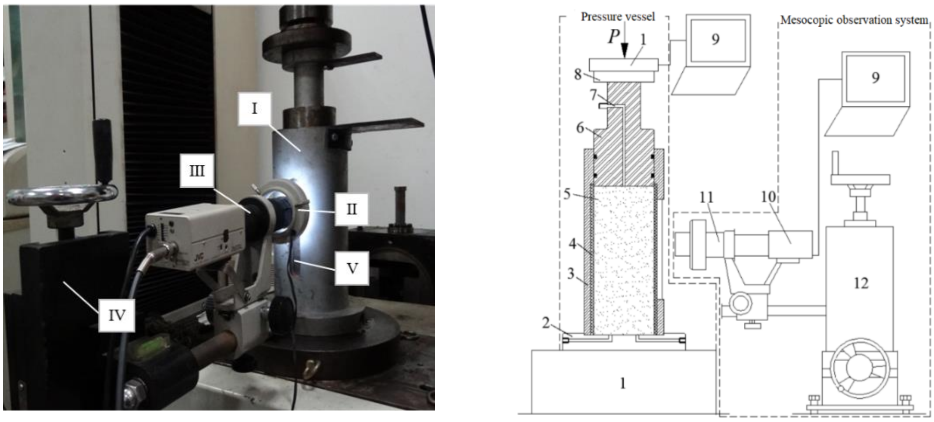

(**a**) (**b**)

Figure 6. Observation apparatus for mesomechanics and deformation of tailings. (**a**) Photo: I. pressure chamber and accessories; II. ring lamp; III. stereomicroscope and charge coupled device camera; IV. 3D movable observation support frame; and V. observation window. (**b**) Schematic [36]: 1. loading indenter; 2. bottom plate; 3. stainless steel cylinder; 4. tempered glass cylinder; 5. tailing specimen; 6. pressure piston; 7. exhaust hole; 8. piston pressure head; 9. computer; 10. charge coupled device video camera; 11. stereoscopic microscope; and 12. 3D movable observation support frame.

According to the actual accumulation condition of tailings in the Huangcaoping tailings pond, the dry density of the samples was set to 1.44 g/cm^3. The degree of saturation of a wet granular material can be calculated by dry density, specific gravity and moisture content, and the calculation formula is as follows:

$$S_r = \frac{\omega G_s}{e} \tag{1}$$

$$e = \frac{\rho_w G_s}{\rho_d} - 1 \tag{2}$$

where S_r is the degree of saturation, G_s is the specific gravity, ω is the moisture content, e is the void ratio, ρ_d is the dry density of specimen, and ρ_w is the density of pure water at 4 °C (1.00 g/cm^3).

The corresponding degrees of saturation of the samples with moisture contents of 9%, 12%, 15%, 18%, and 21% were 42.6%, 56.8%, 71.0%, 85.2%, and 99.4%. During the test, a continuous load was applied to the top surface of the specimens corresponding to the pressure generated by the rising tailings dam.

2.4. Test Steps

(i) Specimen preparation. To ensure the uniformity of the test specimen, according to the test scheme, the tailings samples with a moisture content of 9% were divided into five parts and placed in the pressure chamber (a diameter of 100 mm and height of 200 mm) in sequence. According to the size of the pressure chamber and density of the specimen, the mass and thickness of each layer were calculated to be 493 g and 40 mm, respectively. After each layer of sample was placed in the pressure chamber, a special wooden hammer was used to press the sample to the predetermined thickness. To ensure a natural connection between the two layers of samples, a knife was used to shave the surface of the previous layer of samples; then, the next layer of samples was added. The synthesized specimen was placed in the closed pressure chamber for 24 h before starting the test.

(ii) Pressure chamber and observation system installation. The pressure chamber was placed on the test platform, and the position of the loading test machine indenter was adjusted such that it touches the pressure piston. The stereoscopic microscope and charge coupled device camera were fixed on the 3D movable observation support frame, and the support frame was moved to align the microscope lens and observation window in the pressure chamber. The computer was connected, and the focal length of the lens was adjusted to observe the tailing particles through the image analysis software. Thus, the apparatus was readied for testing, as shown in Figure 6.

(iii) Loading and imaging. A clear observation point was selected, and the initial image of the tailings particle structure in the selected area was imaged. Then, a continuous load was applied at a rate of 0.5 mm/min, and the observation point was continuously tracked by adjusting the observation support frame. Images were captured every 5 min during the test. The maximum load was set to 650 kPa. During the loading process, the exhaust hole remained open, allowing the pore water to drain after saturation. The testing machine automatically stopped applying pressure when the maximum load was attained.

The continuous loading and mesoscopic observation tests of tailings with moisture contents of 12%, 15%, 18%, and 21% were conducted in sequence as per the aforementioned steps.

3. Results and Analysis

3.1. Displacement Deformation Characteristics

The displacement curves of the tailings specimens with different moisture contents under continuous load are shown in Figure 7. A continuous increase in the load causes a nonlinear increase in the settlement displacement. Excluding the curve with 21% moisture content, the behaviors of the pressure−displacement curves under the other four moisture contents are the same. Considering the curve corresponding to 15% moisture content (as shown in Figure 8), the pressure–displacement curve can be broadly divided into four stages:

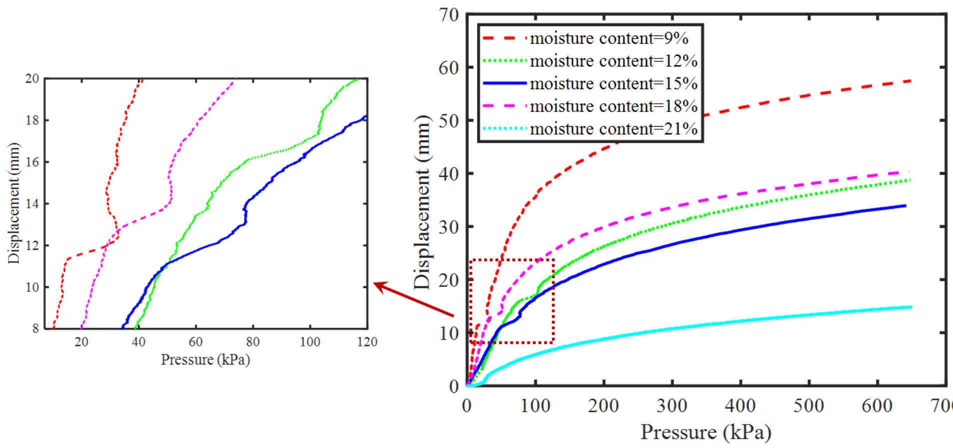

Figure 7. Pressure−displacement curves of tailings specimens with different moisture under continuous load.

The OA segment is the first stage, where the tailings particles are in a loose accumulation state. The settlement displacement increases almost linearly with an increase in pressure. With an increase in displacement, the connection between the particles tightens and cohesion force between the particles increases; however, almost no change is observed along the direction of the particle arrangement.

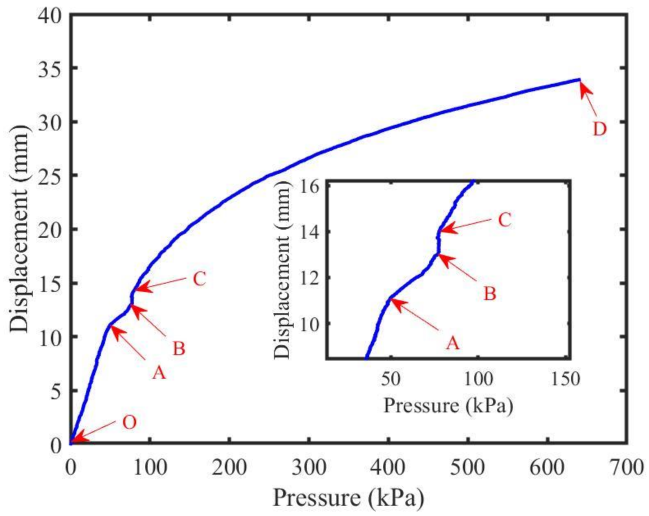

Figure 8. Pressure−displacement curve of tailings specimen with 15% moisture content under continuous load. Points O, A, B, C, and D are the end points or critical points of the curve.

The AB segment is the second stage, where the displacement further increases linearly with an increase in the pressure; however, the slope of the curve is significantly lower than that of the previous stage. Here, the particles are tightly connected, and the cohesion and friction forces between the particles are significantly increased, resulting in a significant increase in the resistance to deformation in the specimen. Furthermore, for the moisture contents of 9%, 12%, 15%, and 18%, the initial pressures are 15.06, 76.1, 48.6, and 31.1 kPa, respectively. The next stage is observed after increments of 16.97, 26.5, 28.43, and 20.21 kPa.

The BC segment is the third stage, where the pressure–displacement curves for all four moisture contents show a vertical steep wall with a length of approximately 1.5 mm. At this stage, the small tailings particles are squeezed into the pores between the large particles, and the particle structure changes, i.e., the relative position of the particles and direction of the particle arrangements change. The initial displacement in this stage with moisture contents of 9%, 12%, 15%, and 18% are 12.32, 17.32, 13.05, and 14.13 mm, respectively. Here, the displacement continues to increase, but the pressure shows a slight downward tendency, indicating that the small particles that squeezed into the large pores are not tightly connected with the surrounding large particles. The friction force between the particles is reduced.

The CD segment is the fourth stage, where the deformation and rate of deformation gradually increase with an increase in the load. Under the action of load, the connections between the rearranged tailings particles gradually tighten and the interaction force between the particles continues to increase, resulting in a gradual increase in the resistance to deformation in the specimen.

As shown in Figure 7, the behavior of the pressure−displacement curve of the specimen with a moisture content of 21% is different from those of the other four specimens. In this curve, there is almost no first stage as described in the aforementioned analysis. The degree of saturation of this specimen was very high, at 99.4%. The specimen attained saturation rapidly under load, and pore water seeping was observed from the exhaust hole of the pressure chamber during the test. Due to the poor permeability of the tailings, the pore water cannot be discharged in time, which leads to the formation of excess pore water pressure. This further reduces the deformation rate and final deformation of the specimen. However, it is possible to clearly observe the particle rearrangement stage where small particles squeeze into the large pores.

The final settlement displacements of the tailings specimens with moisture contents of 9%, 12%, 15%, 18%, and 21% are 57.43, 38.73, 33.93, 40.4, and 14.83 mm, respectively. Although the specimen with 21% moisture content attained saturation rapidly during the compression process, because the pore water did not freely discharge, the final deformation with 21% moisture content was the smallest. As shown in Figure 9, for tailings with a moisture content in the range of 9% to 18%, as the moisture content increased, the final displacement first decreased and then increased, and the final displacement reached the minimum when the moisture content was 15%. Therefore, the specimen with 15% moisture content had the strongest resistance to deformation, that is, 15% is the optimal moisture content of the tailings.

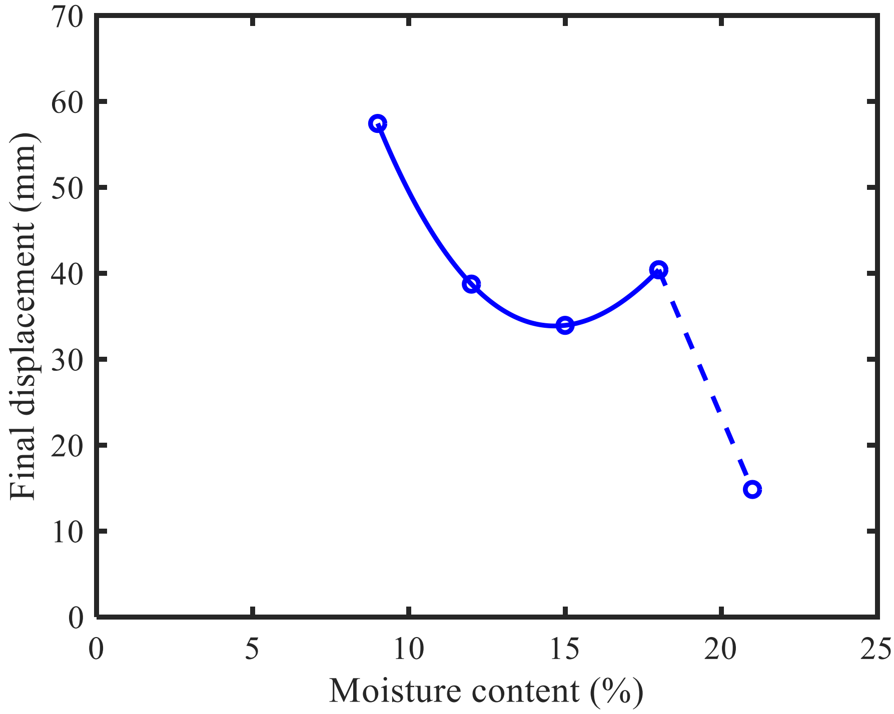

Figure 9. Relation between the final displacement and moisture content.

3.2. Particles Mesostructure Characteristics

During the continuous loading process, changes in the particle mesostructure of the tailings specimen were observed in real time using a stereo microscope and CCD camera; the mesostructure images at different moments were captured. Considering the sample with a moisture content of 15%, the original and binary images of the mesostructure of the tailings particles at different times are shown in Figure 10. The binary images, where the black represents particles and white represents pores, were obtained using the CF2000P polarized light analysis program (manufactured by Shanghai Changfang Optical Instrument Co. Ltd., Shanghai, China). Due to certain unfavorable factors, such as the pore water adhering to the inner wall of the observation window, the movement of particles scratching the observation window, and observation window with a certain curvature instead of a plane, the mesostructure image clarity was reduced.

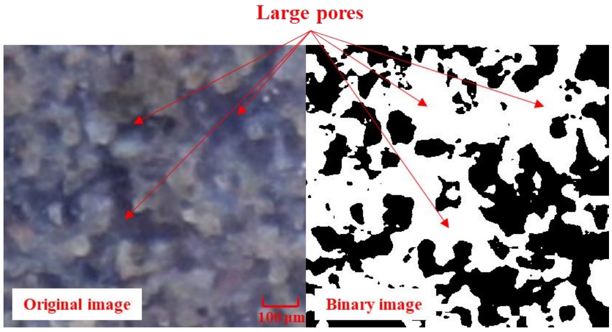

(**a**)

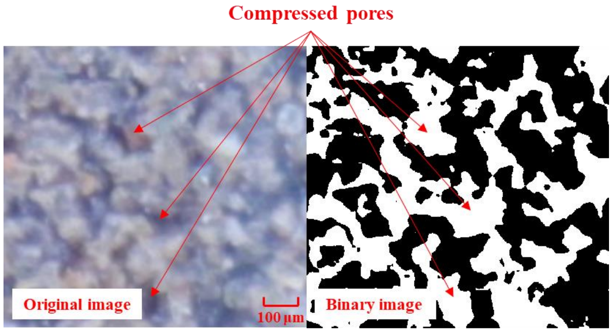

(**b**)

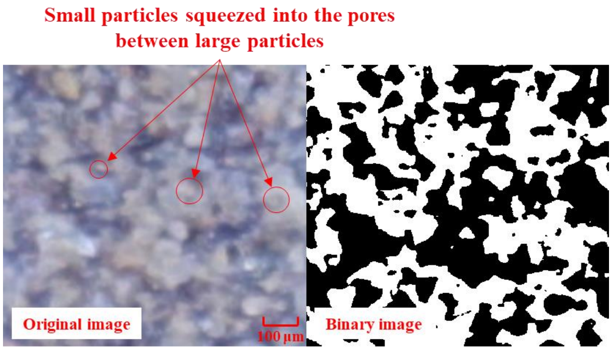

(**c**)

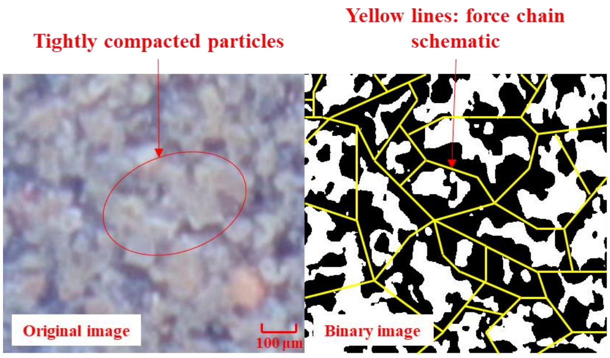

(**d**)

Figure 10. Mesostructure of tailings specimen with 15% moisture content under continuous load: (**a**) 0 s; (**b**) 1500 s; (**c**) 1700 s; (**d**) 3000 s.

The evolution of the particle structure changes the contact force transfer net, viz., the force chain, in the particle system [32,43]. As shown in Figure 10a, when no load is applied, the tailings particle structure presents a loosely dispersed state, the particles are disorderly arranged, and large pores between the particles are clearly visible. As the load increases, the pores are easily compressed, and the connection between the particles tightens, as shown in Figure 10b. The process from the dispersed state of the particles in Figure 10a to the compact state of the particles in Figure 10b corresponds to the OA segment in the pressure−displacement curve in Figure 8. Here, a weak force chain is formed between the particles. With a further increase in the load, there is almost no change in the relative position between the closely connected particles observed in the microscope; however, the macroscopic settlement deformation of the specimen continues to increase, but this increment is small. This shows that a certain amount of elastic deformation may occur at the interconnected parts of the particles, which accumulates to form a macroscopic deformation. This process corresponds to the AB segment of the curve in Figure 8. The force chain between the particles becomes stable and strong. As shown in Figure 10c, when the load increases to a certain extent, the original arrangement and structure of the particles are destroyed, and small particles are squeezed into the pores between large particles, thus reducing the pores between the particles and corresponding BC segment of the pressure−displacement curve. This process generally occurs in binary granular mixtures with large size ratios during volume compression [44,45]. The experimental tailings in this study have a large particle size distribution range with a uniform coefficient of approximately 26, which is a favorable condition for this process. Here, the original force chain between the particles is broken, and the new force chain is not formed. Hence, the load shows less change or may slightly decrease with an increase in the displacement. Then, as the load increases further, the particles are more closely connected, and a more compact structure of the particles is generated, where an extremely stable force chain net is formed, as shown in Figure 10d. Thus, the changes in the mesostructure of the tailings particles can be graphically represented as shown in Figure 11, which are obtained by summarizing the results shown in Figures 8 and 10. The four stages (four thick arrows) shown in Figure 11 correspond to the four stages of the pressure−displacement curve in Figure 8.

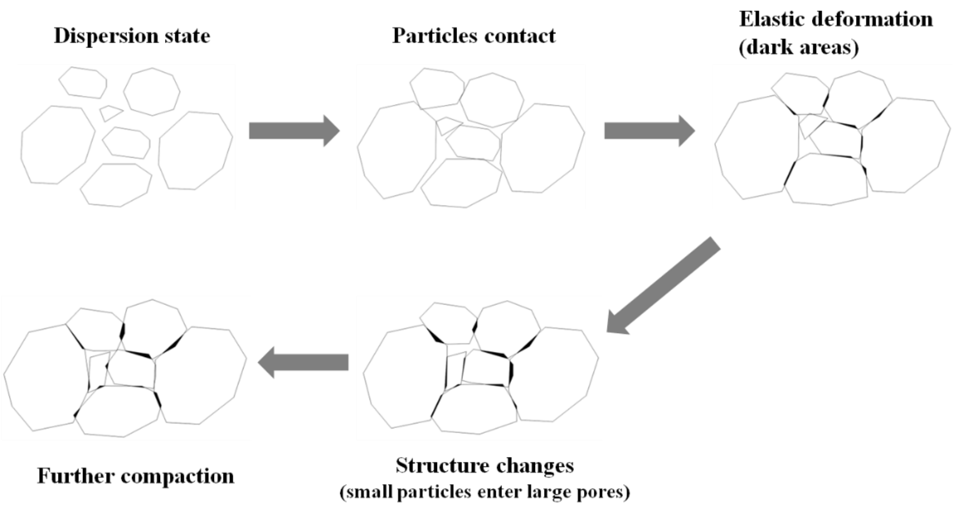

Figure 11. Schematic of mesostructure changes in tailings particles.

4. Discussion

Unsaturated tailings are a three-phase mixture of solid particles, pore water, and pore gas. The liquid between the particles connects the surfaces of adjacent particles; this is called a liquid bridge [40]. The adhesion mode of the pore water to the tailings particles, i.e., the liquid bridge regime, mainly depends on the degree of saturation of the unsaturated tailings [46]. Different liquid bridge regimes exhibit different adhesion force between the particles and their corresponding action mechanism. According to previous research on the liquid bridge regime of wet granular matter [40,46–48], tailings with different degrees of saturation show three different liquid bridge regimes: when the degree of saturation is low (generally less than 10−30%), the liquid bridge is in the pendular regime (Figure 12a); when the tailings are close to saturation (the degree of saturation generally exceeds 70−90%), the liquid bridge is in the capillary regime (Figure 12c); when the degree of saturation is in the middle, the liquid bridge is in a transitional state, which is the funicular regime (Figure 12b).

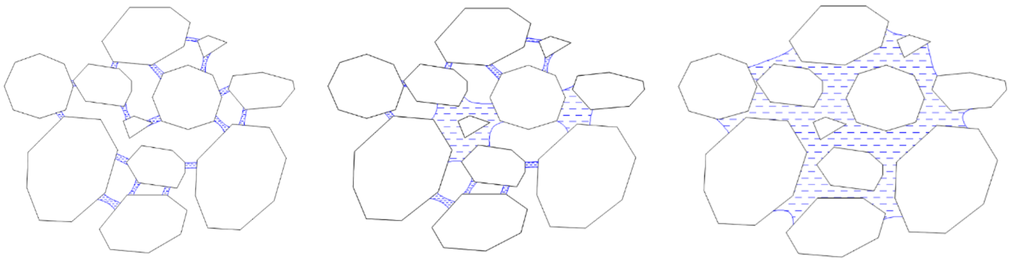

(**a**) (**b**) (**c**)

Figure 12. Liquid bridge regimes in unsaturated and saturated tailings: (**a**) pendular; (**b**) funicular; (**c**) capillary.

For the specimen with a moisture content of 9% in this test, owing to its low degree of saturation (42.6%), its liquid bridge regime is funicular and close to pendular. Here, most of the liquid bridges are very slender and exist around the contact points of the particles. Few pores between the particles are filled with liquid, and the adhesion force of the liquid bridge to the particles is small [49]. Because the moisture content is less than the plastic limit, the pore water exists in the form of firmly bound water, and the specimen is in a solid or semisolid state.

For the specimens with moisture contents of 12%, 15%, and 18%, as the moisture content increased, the degree of saturation of the tailings and proportion of the pores filled with water increased, and the liquid bridge regime gradually changed from funicular to capillary, respectively. Under this condition, the liquid bridge has a strong adhesive force, which can allow several adjacent particles to form a block [50]. Microscopic observation showed that under the action of pressure, the movement of individual particles and overall movement of blocks could be observed. As shown in Figure 13, a block has been translated and rotated integrally, but the relative position of the particles inside the block did not change; however, the structure of the block became compact. A similar phenomenon was observed in the DEM numerical simulation for granular materials, which was conducted by Zdenek Grof et al. [51,52].

When the moisture content exceeds the plastic limit, the tailings specimens are in a plastic state. In addition to firmly bound water around the particles, loosely bound water was existed, which can migrate under the action of squeeze and shear, thereby causing the shape and adhesive force of the liquid bridge to become unstable and demonstrating a lubricating effect. When the moisture content exceeds the liquid limit, a portion of the pore water exists in the form of free water, which further enhances the lubricating effect. Here, the tailings exhibit the flow state; with no lateral pressure restriction, the specimen loses its bearing capacity. Owing to the lubricating effect of the pore water, for the three specimens with moisture contents of 12%, 15%, and 18%, the transition pressure from the OA segment to the AB segment in the pressure−displacement curves (shown in Figures 7 and 8) decreases with an increase in the moisture content. This is consistent with the results reported by Ning Lu et al.—the adhesive force of a liquid bridge is generally maximized in the funicular regime [47,53].

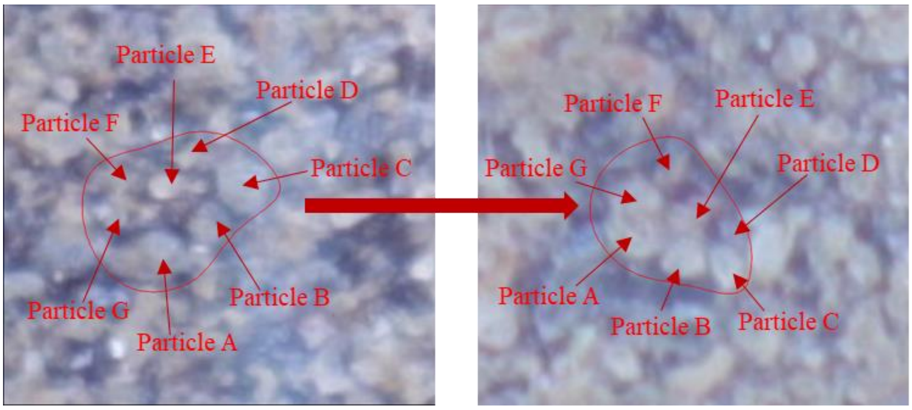

Figure 13. Overall movement of a block.

The specimen with a moisture content of 21% showed a high degree of saturation (99.4%) and attained saturation rapidly owing to volume compression. However, owing to the low permeability of the specimen and high loading rate, the pore water could not be discharged at the appropriate time, resulting in the generation of excess pore water pressure. Excess pore water pressure appears as a force that pushes adjacent particles apart on the mesoscale, which is opposite to the adhesive effect of liquid bridges.

5. Conclusions

In this study, a special testing apparatus was used to study the deformation characteristics and mesostructure evolution mechanism of tailings with different moisture contents under continuous load. The following are the main conclusions:

(1) The mesostructure evolution of unsaturated tailings under continuous load can be divided into four stages: pore compression, elastic deformation, structure change, and further compaction. This is manifested in the macroscopic pressure–displacement curve as a change in the slope of the curve.

(2) When the pressure reaches a certain extent, the original particle arrangements and structure of the specimens are destroyed. Here, the small particles are squeezed into the pores between the large particles; this is observed in the pressure−displacement curve as the continuous increase in displacement under the condition of almost constant pressure.

(3) For unsaturated tailings, there is an optimal moisture content corresponding to the strongest resistance to deformation. The optimal moisture content of the experimental tailings in this study was 15%, which can provide a basis for determining the moisture content of the tailings used in the sub-dam.

(4) The regime of the liquid bridge between the tailings particles varies with the degree of saturation, which further affects the evolution mechanism of the mesostructure of the tailings. Due to the adhesion force of the liquid bridge, the movement of individual particles and overall movement of a block composed of multiple particles were observed in the specimen with a higher degree of saturation.

Author Contributions: Conceptualization, Z.W. and G.H.; data curation, W.G.; formal analysis, W.G., W.W. and X.J.; funding acquisition, W.W., Z.W. and X.J.; investigation, W.G. and W.W.; methodology, W.W.; project administration, Z.W.; resources, Z.W.; supervision, G.H.; validation, W.W. and S.T.; visualization, W.G. and C.J.; writing—original draft, W.G.; writing—review and editing, W.W. All authors have read and agreed to the published version of the manuscript.

Funding: This study was financially supported by the National Natural Science Foundation of China (51804051, 51974051), National Key Research and Development Program of China (2017YFC0804609), Natural Science Foundation of Chongqing, China (cstc2019jcyj-bshX0022, cstc2018jcyjAX0231), and Chongqing Special Postdoctoral Science Foundation (XmT2018017).

Institutional Review Board Statement: Not applicable.

Informed Consent Statement: Not applicable.

Data Availability Statement: The data presented in this study are available on request from the corresponding author. The data are not publicly available due to privacy.

Acknowledgments: The authors would like to thank Qiangui Zhang for his suggestions on the sample preparation and image processing and the reviewers for their constructive comments that improved the paper.

Conflicts of Interest: The authors declare no conflict of interest.

References

1. Kossoff, D.; Dubbin, W.E.; Alfredsson, M.; Edwards, S.J.; Macklin, M.G.; Hudson-Edwards, K.A. Mine Tailings Dams: Characteristics, Failure, Environmental Impacts, and Remediation. *Appl. Geochem.* **2014**, *51*, 229–245. [CrossRef]
2. Vick, S.G. *Planning, Design, and Analysis of Tailings Dams*; BiTech Publishers: Vancouver, BC, Canada, 1990.
3. Rico, M.; Benito, G.; Diez-Herrero, A. Floods from Tailings Dam Failures. *J. Hazard Mater.* **2008**, *154*, 79–87. [CrossRef] [PubMed]
4. Santamarina, J.C.; Torres-Cruz, L.A.; Bachus, R.C. Why Coal Ash and Tailings Dam Disasters Occur: Knowledge Gaps and Management Shortcomings Contribute to Catastrophic Dam Failures. *Science* **2019**, *364*, 526–528. [CrossRef]
5. Van Niekerk, H.J.; Viljoen, M.J. Causes and Consequences of the Merriespruit and Other Tailings-Dam Failures. *Land Degrad. Dev.* **2005**, *16*, 201–212. [CrossRef]
6. Glotov, V.E.; Chlachula, J.; Glotova, L.P.; Little, E. Causes and Environmental Impact of the Gold-Tailings Dam Failure at Karamken, the Russian Far East. *Eng. Geol.* **2018**, *245*, 236–247. [CrossRef]
7. Silva Rotta, L.H.; Alcântara, E.; Park, E.; Negri, R.G.; Lin, Y.N.; Bernardo, N.; Mendes, T.S.G.; Souza Filho, C.R. The 2019 Brumadinho Tailings Dam Collapse: Possible Cause and Impacts of the Worst Human and Environmental Disaster in Brazil. *Int. J. Appl. Earth Obs.* **2020**, *90*, 102119. [CrossRef]
8. Du, Z.; Ge, L.; Ng, A.H.; Zhu, Q.; Horgan, F.G.; Zhang, Q. Risk Assessment for Tailings Dams in Brumadinho of Brazil Using Insar Time Series Approach. *Sci. Total Environ.* **2020**, *717*, 137125. [CrossRef]
9. Thompson, F.; de Oliveira, B.C.; Cordeiro, M.C.; Masi, B.P.; Rangel, T.P.; Paz, P.; Freitas, T.; Lopes, G.; Silva, B.S.; Cabral, A.S.; et al. Severe Impacts of the Brumadinho Dam Failure (Minas Gerais, Brazil) on the Water Quality of the Paraopeba River. *Sci. Total Environ.* **2020**, *705*, 135914. [CrossRef]
10. Armstrong, M.; Petter, R.; Petter, C. Why Have so Many Tailings Dams Failed in Recent Years? *Resour. Policy* **2019**, *63*, 101412. [CrossRef]
11. Wei, Z.A.; Yin, G.Z.; Wang, J.G.; Wan, L.; Li, G.Z. Design, Construction and Management of Tailings Storage Facilities for Surface Disposal in China: Case Studies of Failures. *Waste Manag. Res.* **2013**, *31*, 106–112. [CrossRef]
12. Fredlund, D.G.; Rahardjo, H.; Fredlund, M.D. *Unsaturated Soil Mechanics in Engineering Practice*; John Wiley & Sons: Hoboken, NJ, US, 2012.
13. Zandarin, M.T.; Decop, L.A.; Rodriguez, R.; Zabala, F. The Role of Capillary Water in the Stability of Tailing Dams. *Eng. Geol.* **2009**, *105*, 108–118. [CrossRef]
14. Cao, G.S.; Wang, W.S.; Yin, G.Z.; Wei, Z.A. Experimental Study of Shear Wave Velocity in Unsaturated Tailings Soil with Variant Grain Size Distribution. *Constr. Build. Mater.* **2019**, *228*, 116744. [CrossRef]
15. Ishihara, K.; Ueno, K.; Yamada, S.; Yasuda, S.; Yoneoka, T. Breach of a Tailings Dam in the 2011 Earthquake in Japan. *Soil Dyn. Earthq. Eng.* **2015**, *68*, 3–22. [CrossRef]
16. Pak, A.; Nabipour, M. Numerical Study of the Effects of Drainage Systems on Saturated/Unsaturated Seepage and Stability of Tailings Dams. *Mine Water Environ.* **2017**, *36*, 341–355. [CrossRef]
17. Rico, M.; Benito, G.; Salgueiro, A.R.; Diez-Herrero, A.; Pereira, H.G. Reported Tailings Dam Failures. A Review of the European Incidents in the Worldwide Context. *J. Hazard Mater.* **2008**, *152*, 846–852. [CrossRef]
18. Agurto-Detzel, H.; Bianchi, M.; Assumpcao, M.; Schimmel, M.; Collaco, B.; Ciardelli, C.; Barbosa, J.R.; Calhau, J. The Tailings Dam Failure of 5 November 2015 in se Brazil and Its Preceding Seismic Sequence. *Geophys. Res. Lett.* **2016**, *43*, 4929–4936. [CrossRef]
19. Robertson, P.K.; Melo, L.; Williams, D.J.; Wilson, G.W. Report of the Expert Panel on the Technical Causes of the Failure of Feijão Dam I; 2019. Available online: https://bdrb1investigationstacc.z15.web.core.windows.net/ (accessed on 20 November 2020).
20. Narvaez, B.; Aubertin, M.; Saleh-Mbemba, F. Determination of the Tensile Strength of Unsaturated Tailings Using Bending Tests. *Can. Geotech. J.* **2015**, *52*, 1874–1885. [CrossRef]
21. Robertson, P.K.; da Fonseca, A.V.; Ulrich, B.; Coffin, J. Characterization of Unsaturated Mine Waste: A Case History. *Can. Geotech. J.* **2017**, *54*, 1752–1761. [CrossRef]
22. Zhang, C.; Liu, H.; Yang, C.; Wu, S. Mechanical Characteristics of Non-Saturated Tailings and Dam Stability. *Int. J. Min. Reclam. Environ.* **2017**, *31*, 530–543. [CrossRef]
23. Zhang, F.; Wilson, G.W.; Fredlund, D.G. Estimation of Permeability Function for Bulyanhulu Tailings. *Geotech. Test. J.* **2019**, *42*, 670–686. [CrossRef]
24. Schafer, H.; Beier, N. Estimating Soil-Water Characteristic Curve from Soil-Freezing Characteristic Curve for Mine Waste Tailings Using Time Domain Reflectometry. *Can. Geotech. J.* **2020**, *57*, 73–84. [CrossRef]

25. Fisseha, B.; Bryan, R.; Simms, P. Evaporation, Unsaturated Flow, and Salt Accumulation in Multilayer Deposits of "Paste" Gold Tailings. *J. Geotech. Geoenviron.* **2010**, *136*, 1703–1712. [CrossRef]
26. Li, X.; Li, X.S. Micro-Macro Quantification of the Internal Structure of Granular Materials. *J. Eng. Mech.* **2009**, *135*, 641–656. [CrossRef]
27. Su, H.Z.; Fu, Z.Q.; Gao, A.; Wen, Z.P. Particle Flow Code Method-Based Meso-Scale Identification for Seepage Failure of Soil Levee. *Transp. Porous Med.* **2017**, *119*, 311–336. [CrossRef]
28. Wang, Y.; Li, X.; Zhang, B.; Wu, Y.F. Meso-Damage Cracking Characteristics Analysis for Rock and Soil Aggregate with ct Test. *Sci. China Technol. Sci.* **2014**, *57*, 1361–1371. [CrossRef]
29. Liu, Y.N.; Liu, E.N.; Yin, Z.Y. Constitutive Model for Tailing Soils Subjected to Freeze-Thaw Cycles Based on Meso-Mechanics and Homogenization Theory. *Acta Geotech.* **2020**, *15*, 2433–2450. [CrossRef]
30. Wang, Y.; Li, C.H.; Hu, Y.Z. Use of X-ray Computed Tomography to Investigate the Effect of Rock Blocks on Meso-Structural Changes in Soil-Rock Mixture under Triaxial Deformation. *Constr. Build. Mater.* **2018**, *164*, 386–399. [CrossRef]
31. Xu, W.J.; Hu, L.M.; Gao, W. Random Generation of the Meso-Structure of a Soil-Rock Mixture and Its Application in the Study of the Mechanical Behavior in a Landslide Dam. *Int. J. Min. Sci. Technol.* **2016**, *86*, 166–178. [CrossRef]
32. Zhu, H.X.; Nicot, F.; Darve, F. Meso-Structure Evolution in a 2d Granular Material During Biaxial Loading. *Granul. Matter* **2016**, *18*, 3. [CrossRef]
33. Nguyen, N.S.; Magoariec, H.; Cambou, B.; Danescu, A. Analysis of Structure and Strain at the Meso-Scale in 2d Granular Materials. *Int. J. Solids Struct.* **2009**, *46*, 3257–3271. [CrossRef]
34. Chang, N.; Heymann, G.; Clayton, C. The Effect of Fabric on the Behaviour of Gold Tailings. *Geotechnique* **2011**, *61*, 187–197. [CrossRef]
35. Shi, Y.; Li, C.; Long, D. Study of the Microstructure Characteristics of Three Different Fine-Grained Tailings Sand Samples during Penetration. *Materials* **2020**, *13*, 1585. [CrossRef]
36. Zhang, Q.G.; Yin, G.Z.; Fan, X.Y.; Wei, Z.A.; Wang, W.S.; Nie, W. Loading Capacity and Deformation Characteristics of Tailings Based on a Fractal Geometrical Analysis of the Particle Microstructure. *Minerals* **2015**, *5*, 86–103. [CrossRef]
37. Zhang, Q.G.; Yin, G.Z.; Wei, Z.A.; Fan, X.Y.; Wang, W.S.; Nie, W. An Experimental Study of the Mechanical Features of Layered Structures in Dam Tailings from Macroscopic and Microscopic Points of View. *Eng. Geol.* **2015**, *195*, 142–154. [CrossRef]
38. Chen, Q.; Zhang, C.; Yang, C.; Ma, C.; Pan, Z. Effect of Fine-Grained Dipping Interlayers on Mechanical Behavior of Tailings Using Discrete Element Method. *Eng. Anal. Bound. Elements* **2019**, *104*, 288–299. [CrossRef]
39. Yang, Y.H.; Wei, Z.A.; Fourie, A.; Chen, Y.L.; Zheng, B.B.; Wang, W.S.; Zhuang, S.N. Particle Shape Analysis of Tailings Using Digital Image Processing. *Environ. Sci. Pollut. Res.* **2019**, *26*, 26397–26403. [CrossRef]
40. Sun, Q.C.; Wang, G.Q. *An Introduction to Granular Material Mechanics*; Science Press: Beijing, China, 2009.
41. Ministry of Housing and Urban-Rural Development of the People's Republic of China. *Code for Design of Tailings Facilities*; China Planning Press: Beijing, China, 2013; Volume GB50863-2013.
42. American Society of Testing Materials. *Standard Practice for Classification of Soils for Engineering Purposes (Unified Soil Classification System)*; ASTM International: West Conshohocken, PA, US, 2017; Volume ASTM Standard D2487-17.
43. Pica Ciamarra, M.; Lippiello, E.; Godano, C.; de Arcangelis, L. Unjamming Dynamics: The Micromechanics of a Seismic Fault Model. *Phys. Rev. Lett.* **2010**, *104*, 238001. [CrossRef]
44. Wiacek, J. Geometrical Parameters of Binary Granular Mixtures with Size Ratio and Volume Fraction: Experiments and Dem simulations. *Granul. Matter* **2016**, *18*, 42. [CrossRef]
45. Zhou, W.; Wu, W.; Ma, G.; Ng, T.T.; Chang, X.L. Undrained Behavior of Binary Granular Mixtures with Different Fines Contents. *Powder Technol.* **2018**, *340*, 139–153. [CrossRef]
46. Lappalainen, K.; Manninen, M.; Alopaeus, V.; Aittamaa, J.; Dodds, J. An Analytical Model for Capillary Pressure–Saturation Relation for Gas–Liquid System in a Packed-Bed of Spherical Particles. *Transp. Porous Med.* **2008**, *77*, 17–40. [CrossRef]
47. Lu, N.; Kim, T.H.; Sture, S.; Likos, W.J. Tensile Strength of Unsaturated Sand. *J. Eng. Mech.* **2009**, *135*, 1410–1419. [CrossRef]
48. Kim, T.H.; Sture, S. Capillary-Induced Tensile Strength in Unsaturated Sands. *Can. Geotech. J.* **2008**, *45*, 726–737. [CrossRef]
49. Wang, J.P.; Li, X.; Yu, H.S. Stress-Force-Fabric Relationship for Unsaturated Granular Materials in Pendular States. *J. Eng. Mech.* **2017**, *143*, 04017068. [CrossRef]
50. Wang, J.P.; Gallo, E.; François, B.; Gabrieli, F.; Lambert, P. Capillary Force and Rupture of Funicular Liquid Bridges between Three Spherical Bodies. *Powder Technol.* **2017**, *305*, 89–98. [CrossRef]
51. Grof, Z.; Lawrence, C.J.; Stepanek, F. Computer Simulation of Evolving Capillary Bridges in Granular Media. *Granul. Matter* **2007**, *10*, 93–103. [CrossRef]
52. Grof, Z.; Lawrence, C.J.; Stepanek, F. The Strength of Liquid Bridges in Random Granular Materials. *J. Colloid Interface Sci.* **2008**, *319*, 182–192. [CrossRef]
53. Lu, N.; Godt, J.W.; Wu, D.T. A Closed-Form Equation for Effective Stress in Unsaturated Soil. *Water Resour. Res.* **2010**, *46*, W05515. [CrossRef]